Interfacial Defect Passivation and Charge Carrier Management for Efficient Perovskite Solar Cells via Highly Crystalline Polymer

Rongmei Zhao,[a] Lin Xie,[a,*] Rongshan Zhuang,[a] Tai Wu,[a] Rongjun Zhao,[a] Linqin Wang,[b] Licheng Sun,[b] Yong Hua[a,*]

[a] Yunnan Key Laboratory for Micro/Nano Materials & Technology, School of Materials and Energy, Yunnan University, Kunming 650091, China.

[b] Center of Artificial Photosynthesis for Solar Fuels, School of Science, Westlake University, Hangzhou 310024, China.

Experimental Section

Materials.

Fluorine doped tin oxide (FTO) coated glass substrates, TiO_2 paste, Acetylacetone, Titanium diisoproxide bis(acetylacetonate) 75% in Isopropyl Alcohol, N, N'-dimethylformamide (DMF), dimethyl sulfoxide (DMSO), 4-tert-butylpyridine (tBP), bis(trifluoromethylsulfonyl)imide lithium salt (LiTFSI), Tris(2-(1Hpyrazol-1-yl)-4-tert-butylpyridine)-cobalt(III) tris(bis(trifluoromethyl- sulfonyl) imide) (FK 209), chlorobenzene (CB), acetonitrile (ACN), 2,7-dioctyl[1]benzothieno[3,2-b][1]benzothiophene (C8-BTBT), were purchased from Sigma-aldrich. N^2, N^2, $N^{2'}$, $N^{2'}$, N^7, N^7, $N^{7'}$, $N^{7'}$-octakis(4-methoxyphenyl)-9, 9′-spirobi[9H-fluorene]-2, 2′, 7, 7′-tetramine (Spiro-OMeTAD), Cesium iodide (CsI), formamidiniumiodide (FAI), and methylammonium bromide (MABr) were supplied from greatcell. Lead iodide (PbI_2) and lead bromide ($PbBr_2$) were purchased from TCI Chemicals. All materials were used as received without further purification.

Film and device Fabrication.

Laser patterned FTO substrates (7 Ω per square) were ultrasonically cleaned with running water, detergent, ethanol, and acetone for 20 min in sequence. After drying, a compact TiO_2 layer was deposited on the cleaned FTO glass by spray pyrolysis from a precursor solution of 0.6 mL titanium diisopropoxide bis(acetylacetonate) and 0.4 mL acetylacetonate in 9 mL anhydrous ethanol. After sintering, a mesoporous TiO_2 layer was spin-coated onto the TiO_2 compact layer at 5000 rpm for 20 s, and sintered again. Then, all substrates were transferred to a nitrogen-filled glovebox for perovskite deposition. $(FAPbI_3)_{0.875}(MAPbBr_3)_{0.075}(CsPbI_3)_{0.05}(PbI_2)_{0.03}$ perovskite precursor solution was prepared by dissolving 1.30 M PbI_2, 1.19 M FAI, 0.14 M $PbBr_2$, 0.14 M MABr, and 0.07 M CsI into the DMSO/DMF (1/4 v/v) mixture. The perovskite film was deposited by a consecutively spin-coating process at 2000 rpm for 10 s and 6000 rpm for 30 s on the surface of TiO_2 layer. At the time of 15 s prior to the program end, 100 μL of chlorobenzene was dripped on the spinning substrate, and the film was then annealed at 120°C for 1 h. The target devices were obtained by spin-coating different

concentrations (1, 2, 5, 10, 15 40 mg mL^{-1}, dissolved in chlorobenzene) of C8-BTBT polymer at 4500 rpm for 30 s. Subsequently, the Spiro-OMeTAD was spin-coated onto the perovskite/C8-BTBT films at 4500 rpm for 30 s using 69.36 mM of Spiro-OMeTAD in CB with additives of 28.8 μL *t*-BP, 17.8 μL LiTFSI (520 mg mL^{-1} in ACN), 6.5 μL FK209 (300 mg mL^{-1} in ACN). Finally, a gold layer was thermally evaporated under a lower vacuum ($\leqslant 2\times10^{-4}$ Pa) to complete the device fabrication.

Film and device characterizations.

The UV-vis absorption spectra were recorded by a spectrophotometer (UV-2600, Shimadzu). The Normalized differential pulse voltammetry (DPV) was measured by Electrochemical Workstation (Zennium X, Zahner). Current density-voltage characteristics were measured under 100 mW cm^{-2} (AM 1.5G illumination) using a Newport solar simulator (model 91160) and a Keithley 2400 source/meter. The external quantum efficiency (EQE) spectra were recorded using a computer-controlled setup consisting of a Xenon light source (Spectral Products ASB-XE-175), a monochromator (Spectra Products CM110), and a potentiostat (LabJack U6 DAQ board), calibrated by a certified reference solar cell (Fraunhofer ISE). The steady-state photoluminescence (PL) measurement was performed using a spectrometer (FLS1000, Edinburgh Instruments). The time-resolved PL (TRPL) decay transients were measured using a picosecond pulse diode laser (EPL-470). Nanosecond transient absorption (TA) spectroscopy was investigated by a spectrometer (LP980, Edinburgh Instruments). The space-charge limited current (SCLC) measurements were performed by collecting the *I–V* characteristics of devices in dark conditions. The surface morphology of films was characterized by scanning electron microscopy (SEM) and atomic force microscope (AFM) with the tapping mode. X-ray diffraction (XRD) patterns of films were measured with a TTR-18KW diffractometer, with Cu Kα radiation (λ= 0.15405 nm) operated at 10000 W power (40 kV, 250 mA). X-ray photoelectron spectroscopy (XPS) was performed using a scanning XPS microprobe ($K^{-}Alpha^{+}$). Femtosecond transient absorption (fs-TA) measurements were performed for the films by using amultipass

amplified Ti: sapphire laser (800 nm laser pulses with a 3.5 m*J*/pulse; pulse width of ~120 fs with a repetition rate of 2 kHz, Astrella from Coherent; the detection time delay is in the range of 8.5 ns in conjunction with Helios spectrometers. Excitation pump pulses were generated after passing through a fraction of the 800 nm beam into a spectrally tunable (240–2600 nm) optical parametric amplifier (Newport Spectra-Physics). The probe pulses (UV-Visible and NIR wavelength continuum, white light) were generated by passing another fraction of the 800 nm pulses through a 2 mm thick calcium fluoride (CaF_2) crystal. All the fs-TA experiments were performed under identical ambient conditions at room temperature. Grazing-incidence wide-angle X-ray scattering (GIWAXS) was performed on a Duo microsourced single-crystal X-ray diffractometer (Bruker D8 Venture) with Photon III detector and Cu-Diamond X-ray sources (λ= 1.5406 Å). The data reduction was processed using APEX3 software. The Fourier-transform infrared spectroscopy (FTIR) spectroscopy was carried out using Nicolet iS10 (Thermo Fisher). The Raman spectroscopy was measured by Confocal Raman Microscope (InVia, Renishaw). A Mettler heating stage (FP 82 HT) was used for polarizing optical microscopy (POM, Optiphot 2, Nikon) and DSC were recorded with a DSC 200 F3 Maia calorimeter (NETZSCH) at 10 K min^{-1}.

SCLC measurement

Hole mobility

Fluorine doped tin oxide (FTO) glass was patterned via laser etching for the fabrication of a hole-only device. The clean FTO glasses were cleaned by ozone treatment again. The PEDOT:PSS layer was spin-coated onto the substrate at 4000 rpm for 30s and annealed at 170°C for 20 min in air. After cooling, the glasses were transferred to the nitrogen-filled glovebox. A film of C8-BTBT, Spiro-OMeTAD and Spiro-C8 was spun at 4500 rpm for 30 s, respectively. The gold layer was finally evaporated density-voltage (*J-V*) curve of a hole-only device was measured with a Keithley 2400 source-measure unit in a nitrogen-filled glovebox.

The hole mobility was derived by fitting *J–V* curve with Mott-Gurney equation[1]:

$$J = \frac{9}{8}\varepsilon_0\varepsilon_r\mu\frac{V^2}{L^3}$$

where J is the current density. ε_0 is the vacuum permittivity. ε_r is the relative dielectric constant of the material. μ is the hole mobility. L is the thickness of the hole transport layer. V is the applied voltage.

Trap density

The measurement of the trap density (n_{trap}) is the same as the above method with the structure of 1) "hole only" device: FTO/PEDOT:PSS/perovskite/HTM/Au; 2) "electron only" device: FTO/PCBM/perovskite/PCBM/Au. The n_{trap} was estimated using the following equation[2]:

$$n_{trap} = \frac{2\varepsilon\varepsilon_0 V_{TFL}}{eL^2}$$

where, V_{TFL} is the trap-filled limit (TFL) voltage, ε is the dielectric constant of the perovskite layer. ε_0 is the vacuum permittivity. e is the charge. L is the thickness of the perovskite layer.

TRPL analysis

The TPRL results are fitted through the biexponential equation as below:

$$\mathrm{f(t)} = A_1 \exp\left(\frac{-t}{\tau_1}\right) + A_2 \exp\left(\frac{-t}{\tau_2}\right)$$

And the average value of lifetime ($\tau_{ave.}$) is calculated by the following equation:

$$\tau_{ave.} = \frac{A_1 * \tau_1^2 + A_2 * \tau_2^2}{A_1 * \tau_1 + A_2 * \tau_2}$$

τ_1 and τ_2 represent the fast and slow decay times, which are derived from the charge carriers quenching and the radiative recombination, respectively[3-4].

TA analysis

The TA results are fitted with the biexponential decay function as below:

$$\mathrm{y} = A_1 \exp\left(\frac{-t}{\tau_1}\right) + A_2 \exp\left(\frac{-t}{\tau_2}\right) + y_0$$

And the average value of lifetime ($\tau_{ave.}$) is calculated by the following equation:

$$\tau_{ave.} = \frac{A_1 * \tau_1^2 + A_2 * \tau_2^2}{A_1 * \tau_1 + A_2 * \tau_2}$$

τ_1 and τ_2 represent the fast and slow decay times.[5]

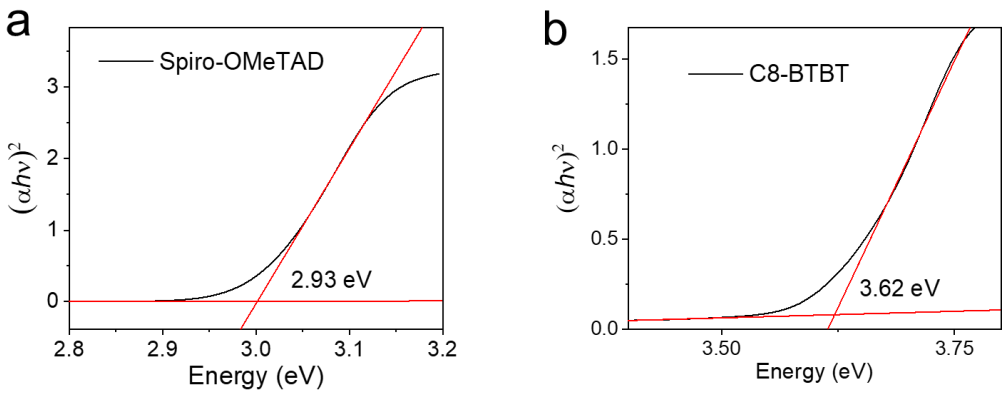

Figure S1. Tauc plots of different solutions in CH_2Cl_2, a) Spiro-OMeTAD and b) C8-BTBT.

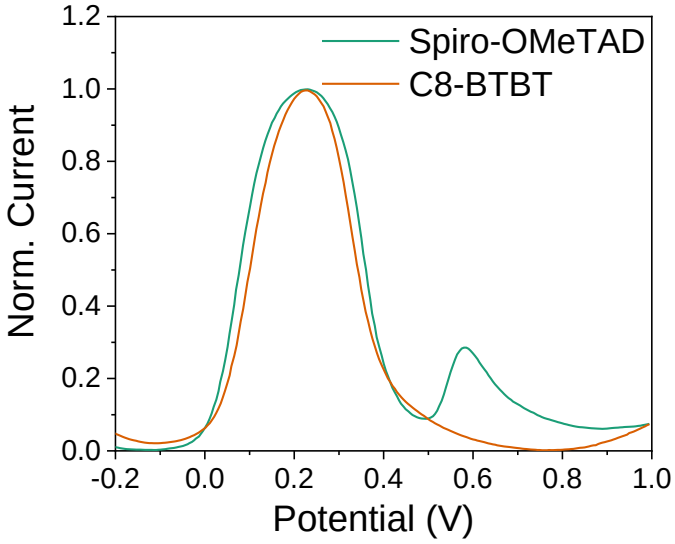

Figure S2. Normalized differential pulse voltammetry (DPV) spectra of Spiro-OMeTAD and C8-BTBT solution in CH_2Cl_2.

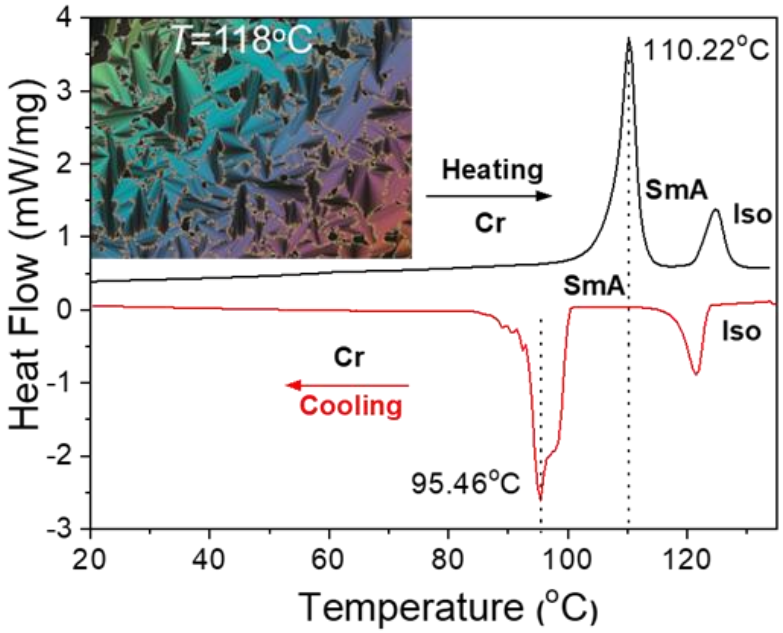

Figure S3. DSC heating and cooling scans (10 K min^{-1}) of bare C8-BTBT powder. Cr = crystalline solid; SmA = Smectic phase; Iso = isotropic liquid state. (Insert: POM textures of smectic liquid crystal under the cross polarizer).

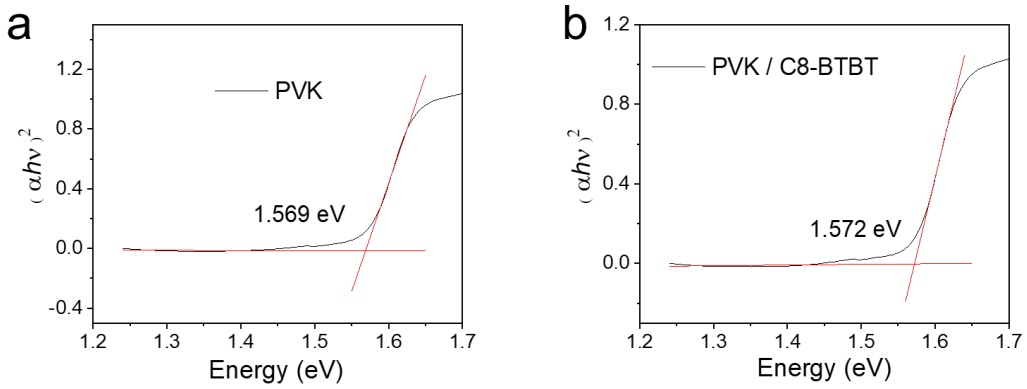

Figure S4. Tauc plots of a) perovskite film and b) perovskite/C8-BTBT film.

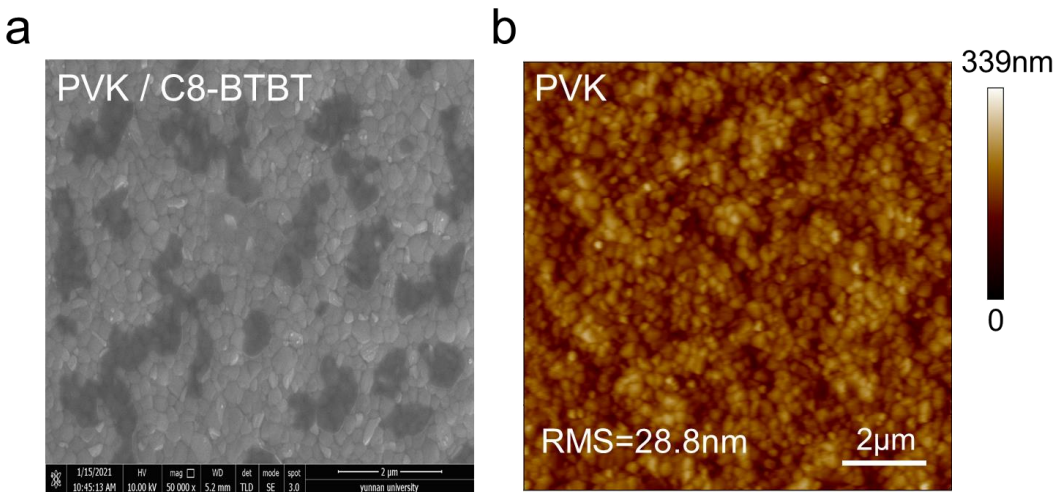

Figure S5. a) The SEM image of C8-BTBT on the surface of perovskite film, b) AFM image of bare perovskite film.

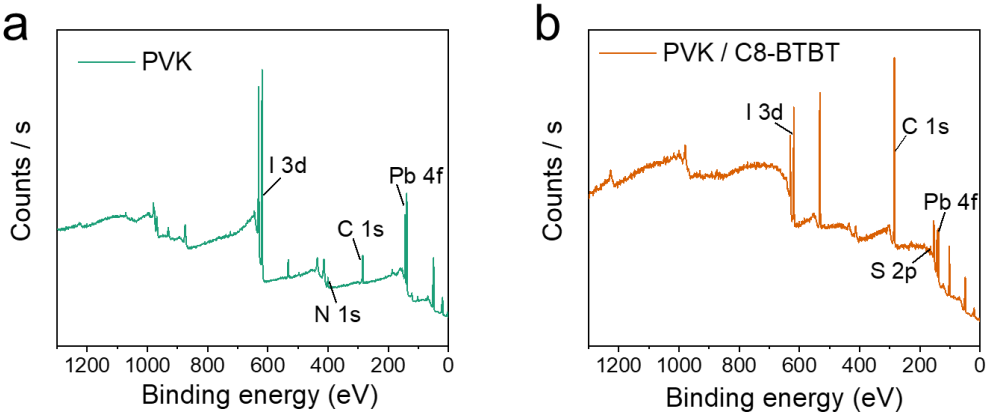

Figure S6. Full XPS spectra of a) perovskite film, b) C8-BTBT prepared on perovskite film.

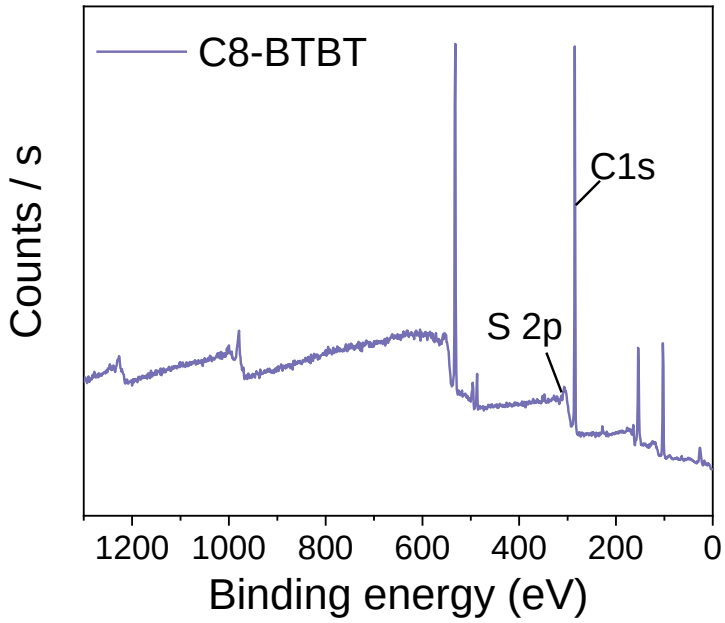

Figure S7. Full XPS spectra of bare C8-BTBT film.

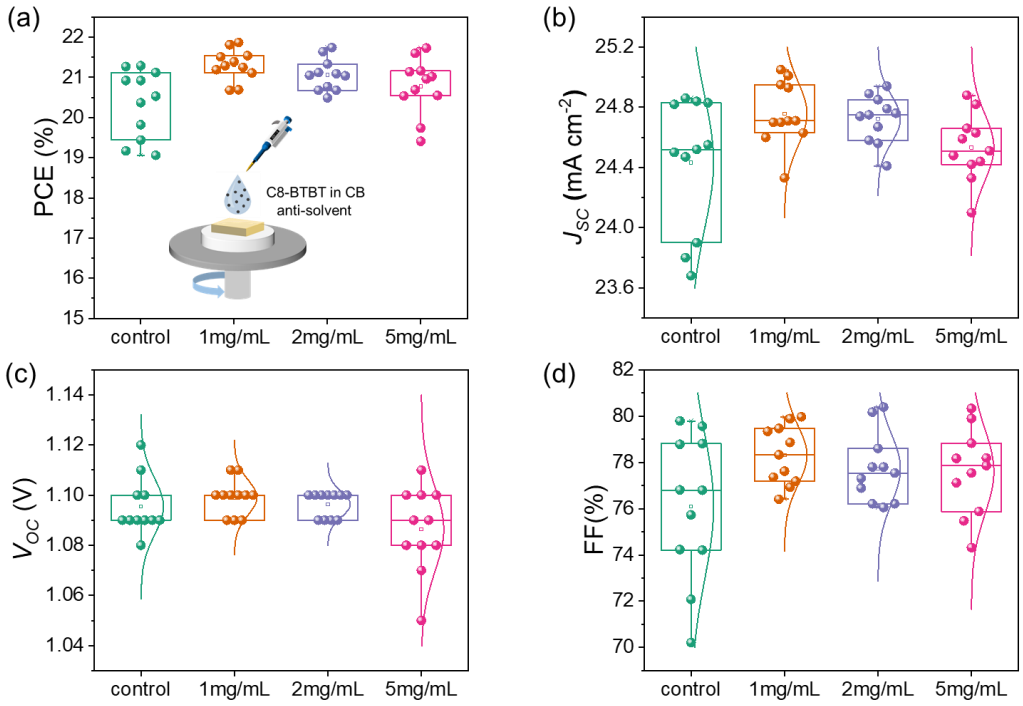

Figure S8. Statistics on photovoltaic parameters of a) PCE, b) J_{SC}, c) V_{OC} and d) FF depending on the various concentration of C8-BTBT anti-solvent modified devices.

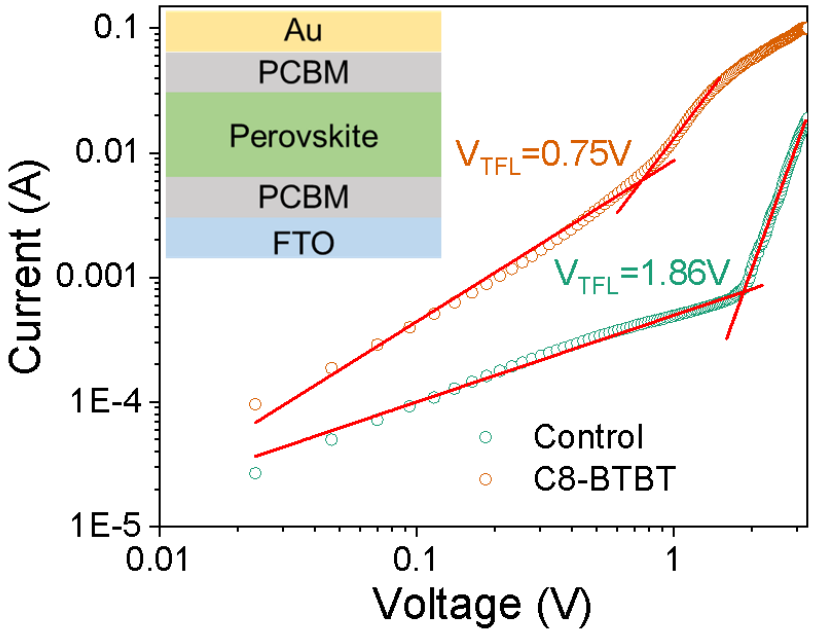

Figure S9. Dark $J-V$ curves of control and C8-BTBT antisolvent modified devices.

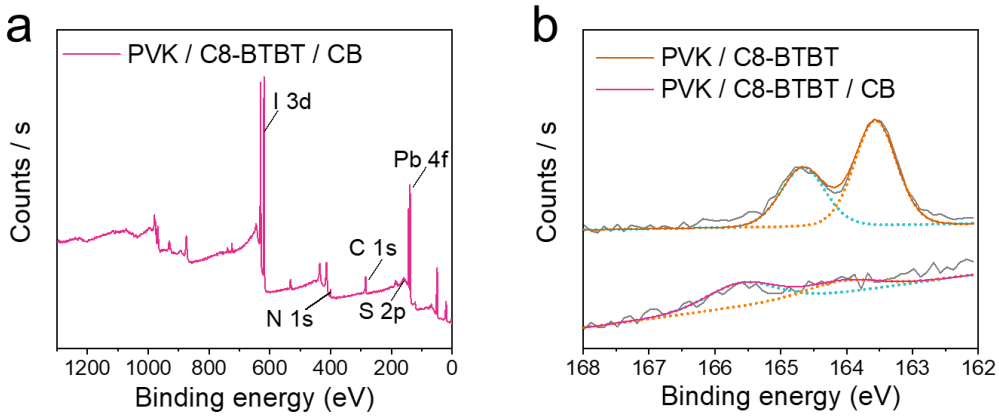

Figure S10. a) Full XPS spectra of C8-BTBT modified perovskite film washed by pure CB solvent, and b) XPS core-level spectra of S 2p in C8-BTBT modified perovskite film with and without CB washing.

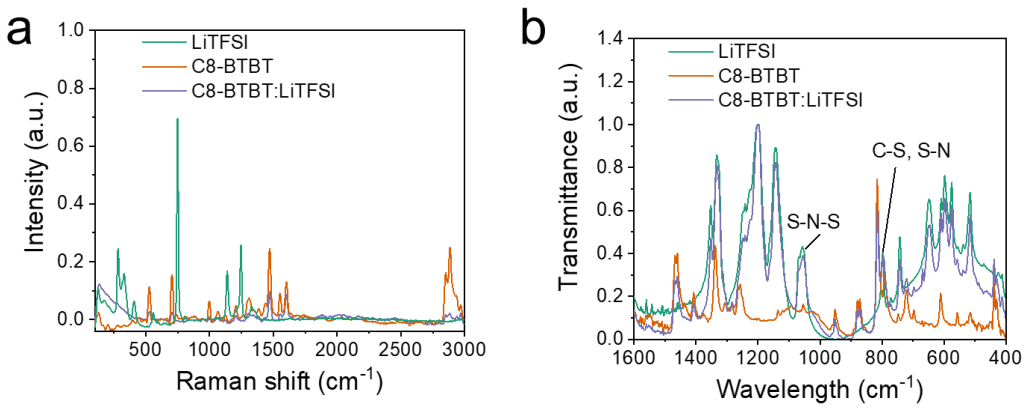

Figure S11. a) Raman Spectra and b) FTIR spectra of the mixture of C8-BTBT and LiTFSI, LiTFSI and C8-BTBT powders, respectively.

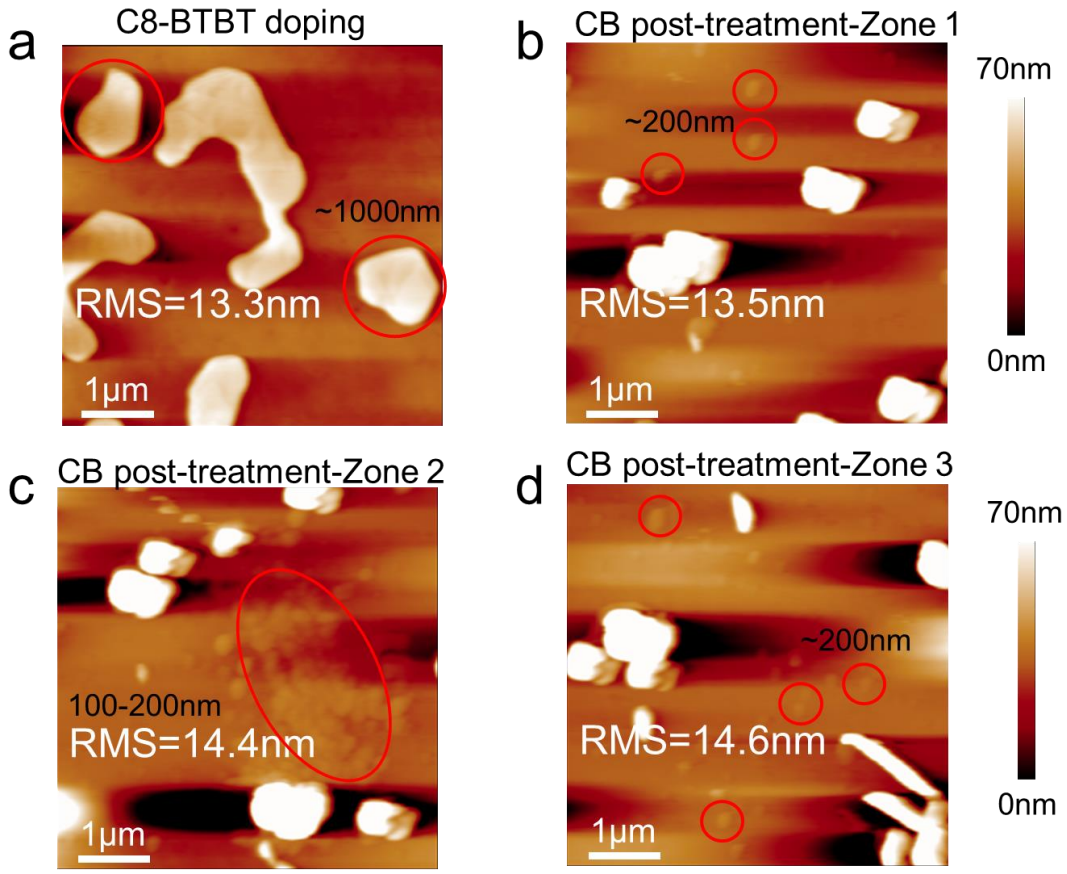

Figure S12. AFM image of a) C8-BTBT doped Spiro-OMeTAD film, b-d) AFM images of C8-BTBT doped Spiro-OMeTAD film in different areas after CB post-treatment.

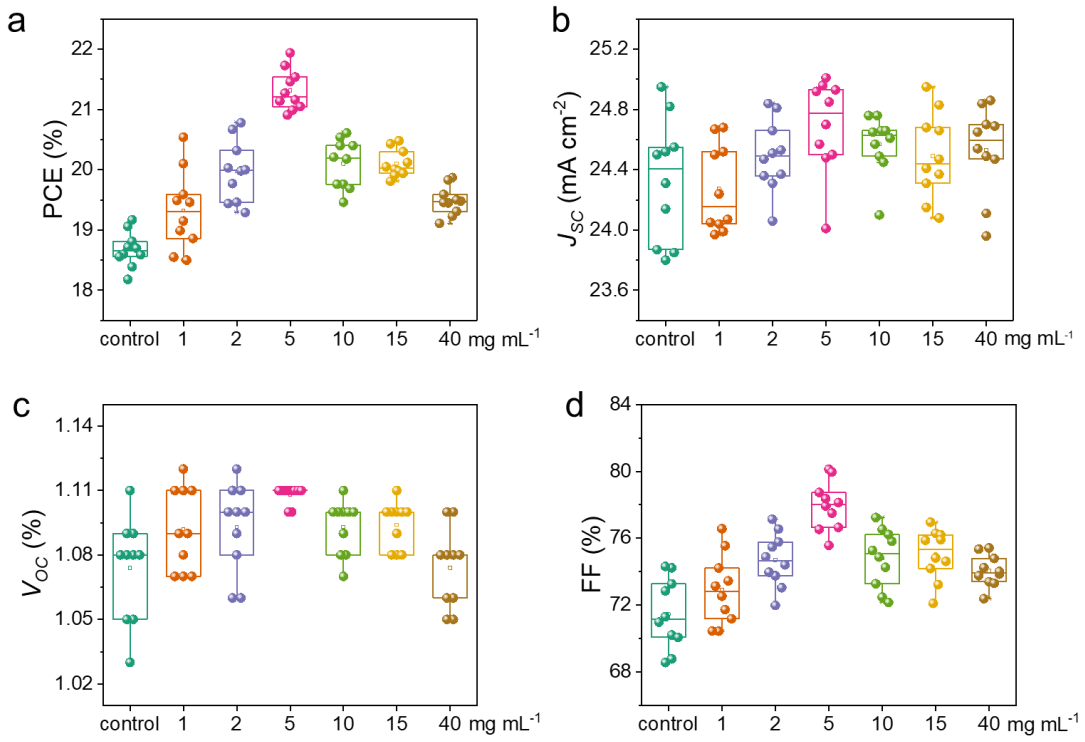

Figure S13. Statistics on photovoltaic parameters of (a) PCE, (b) J_{SC}, (c) V_{OC}, and (d) FF modified with and without various concentrations of C8-BTBT based on 10 devices.

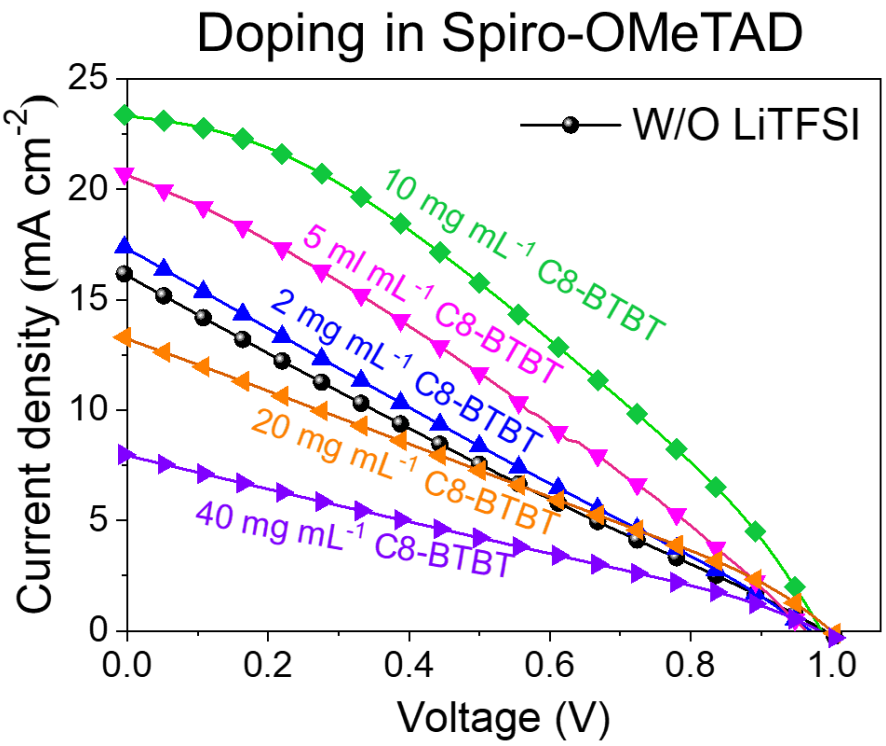

Figure S14. The current density-voltage (*J-V*) curves of the devices with different concentrations of C8-BTBT doped Spiro-OMeTAD (without LiTFSI dopants).

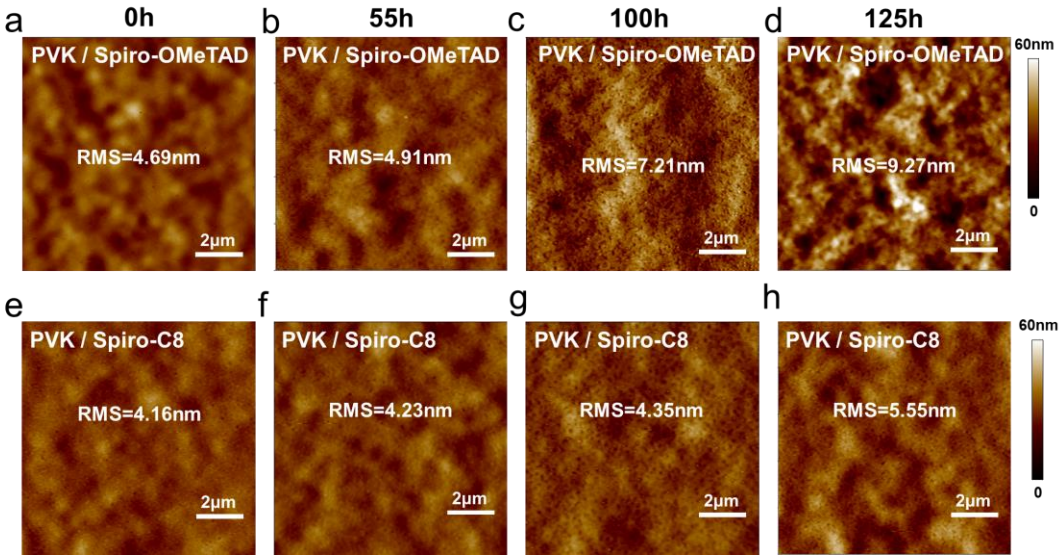

Figure S15. The AFM images of (a-d) Spiro-OMeTAD and (e-h) Spiro-C8 on top of perovskite films at 65°C in different periods.

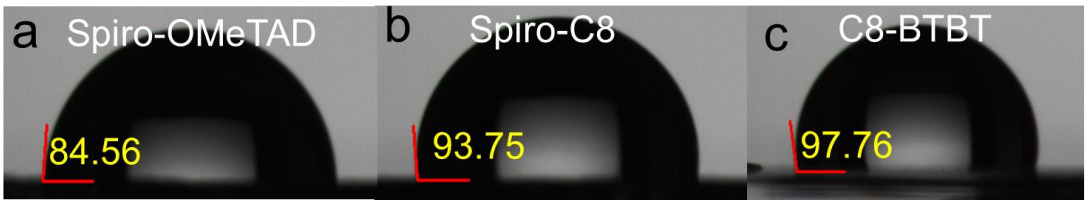

Figure S16. The water contact angle measurement of Spiro-OMeTAD, Spiro-C8 and C8-BTBT on perovskite films, respectively.

Table S1. Fitted results of TRPL decay curves in Figure 2f.

Films	A_1	τ_1 (ns)	A_2	τ_2 (ns)	$\tau_{ave.}$(ns)
Glass/perovskite	0.76	12.9	0.24	242.9	209.2
Glass/perovskite/C8-BTBT	0.95	5.3	0.05	353.2	279.2

Table S2. The corresponding photovoltaic parameters (reverse scan) for the control and C8-BTBT-antisolvent modified devices (two-step), measured under AM 1.5 illumination.

Device	J_{SC} (mA cm^{-2})	V_{OC} (V)	FF (%)	PCE (%)
Control	24.43 ± 0.44	1.09 ± 0.011	76.09 ± 3.15	20.35 ± 0.85
1mg mL^{-1}	24.76 ± 0.21	1.10 ± 0.007	78.31 ± 1.27	21.30 ± 0.38
2 mg mL^{-1}	24.72 ± 0.15	1.09 ± 0.005	77.72 ± 1.49	21.06 ± 0.39
5 mg mL^{-1}	24.53 ± 0.22	1.09 ± 0.016	77.60 ± 1.83	20.78 ± 0.70

Table S3. Fitted results of TRPL decay curves in Figure 3b for perovskite, perovskite/Spiro-OMeTAD, perovskite/Spiro-C8 films on FTO/TiO_2 surface, respectively.

Films	A_1	τ_1 (ns)	A_2	τ_2 (ns)	$\tau_{ave.}$(ns)
perovskite	0.28	4.4	0.72	122.5	120.9
perovskite/Spiro-OMeTAD	0.70	3.1	0.30	37.6	31.9
perovskite/Spiro-C8	0.80	3.3	0.20	37.8	28.7

Table S4. The average photovoltaic parameters of devices modified with C8-BTBT and without C8-BTBT based on 10 devices for each sample.

Device	J_{SC} (mA cm^{-2})	V_{OC} (V)	FF (%)	PCE (%)
Control	24.33 ± 0.41	1.07 ± 0.024	71.46 ± 2.12	18.68 ± 0.29
1 mg mL^{-1}	24.27 ± 0.29	1.09 ± 0.019	72.93 ± 2.08	19.32 ± 0.65
2 mg mL^{-1}	24.49 ± 0.24	1.09 ± 0.021	74.70 ± 1.59	19.97 ± 0.51
5 mg mL^{-1}	24.69 ± 0.31	1.11 ± 0.004	77.95 ± 1.46	21.32 ± 0.34
10 mg mL^{-1}	24.57 ± 0.19	1.09 ± 0.013	74.82 ± 1.74	20.10 ± 0.40
15 mg mL^{-1}	24.49 ± 0.28	1.09 ± 0.011	75.02 ± 1.53	20.10 ± 0.23
40 mg mL^{-1}	24.53 ± 0.29	1.07 ± 0.018	74.05 ± 0.95	19.48 ± 0.24

Table S5. Optimal photovoltaic parameters of the PSCs devices with different concentrations of C8-BTBT doped Spiro-OMeTAD (without LiTFSI dopants).

Device	J_{SC} (mA cm^{-2})	V_{OC} (V)	FF (%)	PCE (%)
W/O LiTFSI	19.47	0.99	19.58	3.78
2 mg mL^{-1}	20.55	0.97	21.00	4.19
5 mg mL^{-1}	22.41	0.96	27.09	5.85
10 mg mL^{-1}	23.69	0.99	34.13	7.97
20 mg mL^{-1}	15.45	1.00	23.74	3.67
40 mg mL^{-1}	9.51	0.98	22.68	2.12

References

1. Rodriguez-Seco, C.; Mendez, M.; Roldan-Carmona, C.; Cabau, L.; Asiri, A. M.; Nazeeruddin, M. K.; Palomares, E., Benzothiadiazole Aryl-amine Based Materials as Efficient Hole Carriers in Perovskite Solar Cells. *ACS Appl Mater Interfaces* **2020**, *12*, 32712-32718.

2. Hu, X.; Wang, H.; Wang, M.; Zang, Z., Interfacial defects passivation using fullerene-polymer mixing layer for planar-structure perovskite solar cells with negligible hysteresis. *Solar Energy* **2020**, *206*, 816-825.

3. Chen, J.; Zhang, C.; Liu, X.; Peng, L.; Lin, J.; Chen, X., Carrier dynamic process in all-inorganic halide perovskites explored by photoluminescence spectra. *Photonics Res.* **2021**, *9*, 151-170.

4. Jiang, T.; Chen, Z.; Chen, X.; Chen, X.; Xu, X.; Liu, T.; Bai, L.; Yang, D.; Di, D.; Sha, W. E. I.; Zhu, H.; Yang, Y. M., Power Conversion Efficiency Enhancement of Low-Bandgap Mixed Pb–Sn Perovskite Solar Cells by Improved Interfacial Charge Transfer. *ACS Energy Lett.* **2019**, *4*, 1784-1790.

5. Yu, W.; Li, F.; Wang, H.; Alarousu, E.; Chen, Y.; Lin, B.; Wang, L.; Hedhili, M. N.; Li, Y.; Wu, K.; Wang, X.; Mohammed, O. F.; Wu, T., Ultrathin Cu_2O as an efficient inorganic hole transporting material for perovskite solar cells. *Nanoscale* **2016**, *8*, 6173-6179.